Spatiotemporal activation of the C/EBPβ/δ-secretase axis regulates the pathogenesis of Alzheimer's disease

Hualong Wang[a,b,c], Xia Liu[a], Shengdi Chen[b,1], and Keqiang Ye[a,d,1]

[a]Department of Pathology and Laboratory Medicine, Emory University School of Medicine, Atlanta, GA 30322; [b]Department of Neurology, Ruijin Hospital, Shanghai Jiaotong University School of Medicine, 200025 Shanghai, People's Republic of China; [c]Department of Neurology, The First Hospital of Hebei Medical University, 050031 Shijiazhuang, Hebei, People's Republic of China; and [d]Tongji Hospital, Tongji University School of Medicine, 200120 Shanghai, People's Republic of China

Edited by Solomon H. Snyder, Johns Hopkins University School of Medicine, Baltimore, MD, and approved November 16, 2018 (received for review September 14, 2018)

Alzheimer's disease (AD) neuropathological hallmarks include senile plaques with aggregated amyloid beta as a major component, neurofibrillary tangles (NFT) containing truncated and hyperphosphorylated Tau, extensive neuronal loss, and chronic neuroinflammation. However, the key molecular mechanism that dominates the pathogenesis of AD remains elusive for AD. Here we show that the C/EBPβ/δ-secretase axis is activated in an age-dependent manner in different brain regions of the 3×Tg AD mouse model, elevating δ-secretase–truncated APP and Tau proteolytic truncates and promoting senile plaques and NFT formation in the brain, associated with gradual neuronal loss and chronic neuroinflammation. Depletion of inflammatory cytokine-regulated transcription factor C/EBPβ from 3×Tg mice represses APP, Tau, and δ-secretase expression, which subsequently inhibits APP and Tau cleavage, leading to mitigation of AD pathologies. Knockout of δ-secretase from 3×Tg mice strongly blunts AD pathogenesis. Consequently, inactivation of the C/EBPβ/δ-secretase axis ameliorates cognitive dysfunctions in 3×Tg mice by blocking APP and Tau expression and their pathological fragmentation. Thus, our findings support the notion that C/EBPβ/δ-secretase axis plays a crucial role in AD pathogenesis.

neurodegenerative diseases | Alzheimer's disease | C/EBPβ | δ-secretase | AEP

Alzheimer's disease (AD) is the leading cause of dementia in the elderly with age being the biggest risk factor. It is the most common neurodegenerative disease with a progressive decline in cognitive functions. The prominent pathological features include extracellular deposit of amyloid beta (Aβ) aggregates, also called "senile plaques" with Aβ peptides as major components and intraneuronal neurofibrillary tangles (NFTs) that mainly contain filamentous inclusion of hyperphosphorylated and truncated Tau, a microtubule-associated cytoskeletal protein. Moreover, AD is also associated with extensive neuronal cell loss in the brain regions responsible for memory, language, and other functions. Furthermore, the AD brain is affected with chronic neuroinflammation associated with massive microglia activation (1). The amyloid hypothesis that postulates Aβ is the causative agent in AD has dominated the field research and therapeutic drug development for decades (2). There are mounting arguments both for and against the hypothesis. The amyloid cascade hypothesis has led to a number of therapeutic approaches, all of which, to date, have failed to reach their primary efficacy end points in clinical trials (3). The failure of clinical trials targeting Aβ by Aβ immunization and BACE1 inhibitors argues against this hypothesis (4, 5). However, Musiek and Holtzman (6) recently proposed that Aβ acts primarily as a trigger of other downstream processes, particularly Tau aggregation, which mediate neurodegeneration. Aβ appears to be necessary, but not sufficient, to cause AD, and its major pathogenic effects may occur very early in the disease process.

Asparagine endopeptidase (AEP), also called "legumain," is a lysosomal cysteine peptidase that specifically cleaves the substrates after asparagine, and this enzymatic activity is tightly regulated by pH (7). AEP is activated under acidosis. It is upregulated during hypoxia and inflammation (8, 9). Previously, we showed that this enzyme is activated in the brain during stroke, cleaving at the N175 residue of SET, a DNase inhibitor and PP2A inhibitor. Cleavage of SET by AEP induces neuronal cell death by triggering genomic DNA nicking (10). Moreover, this process also elicits Tau hyperphosphorylation by inhibiting PP2A, a major Tau phosphatase (8). Recently, we found that AEP cuts Tau at the N255 and N368 residues, promoting its aggregation and neurotoxicities. Knockout of AEP from Tau P301S mice alleviates Tau pathologies and restores the cognitive functions (11). Further, we reported that AEP acts as a δ-secretase by truncating APP at N373 and N585 residues, and the resultant C-terminal fragment, C586–695, is more readily cleaved by BACE1 to enhance Aβ generation. Knockout of δ-secretase from 5×FAD mice diminishes senile plaque deposition, mitigating synaptic plasticity and improving cognitive functions (12). δ-Secretase is positively regulated by SRPK2 phosphorylation on the S226 residue, promoting its enzymatic activity (13), and is negatively regulated by Akt phosphorylation on the T322 residue, blocking its proteolytic activation (14). Via high-throughput screening we have identified an orally bioactive and brain-permeable small molecule that displays promising therapeutic efficacy in various AD mouse models by selectively blocking δ-secretase (15), supporting the notion that

Significance

Our most recent reports demonstrate that δ-secretase (AEP) cleaves both APP and Tau, promoting Ab and neurofibrillary tangle formation. Depletion of δ-secretase diminishes Alzheimer's disease (AD) pathologies and restores cognitive functions in AD mouse models. Moreover, we found that C/EBPβ, an inflammatory cytokine or Ab-activated transcription factor, dictates δ-secretase expression during aging. Overexpression of C/EBPβ facilitates AD pathologies via upregulating δ-secretase, whereas depletion of C/EBPβ reduces AD pathologies. In the current study, we examined the pathological roles of the C/EBPβ/δ-secretase axis in different AD mouse models, at different time points, and in different brain regions and found that this pathway plays a critical role in mediating AD pathologies and cognitive function. Hence, C/EBPβ/δ-secretase spatiotemporally mediates AD pathogenesis.

Author contributions: S.C. and K.Y. designed research; H.W. performed research; X.L. contributed new reagents/analytic tools; H.W. analyzed data; and S.C. and K.Y. wrote the paper.

The authors declare no conflict of interest.

This article is a PNAS Direct Submission.

[1]To whom correspondence may be addressed. Email: ruijincsd@126.com or kye@emory.edu.

This article contains supporting information online at www.pnas.org/lookup/suppl/doi:10.1073/pnas.1815915115/-/DCSupplemental.

Published online December 10, 2018.

δ-secretase is an attractive drug target for treating AD. Most recently, we show that δ-secretase is augmented in the brain in an age-dependent way that is primarily dictated by a transcription factor, C/EBPβ (CCAAT-enhancer–binding protein β) (16), which is activated by inflammatory cytokines (17–19) and by Aβ (20) as well. Overexpression of C/EBPβ facilitates AD pathologies by up-regulating δ-secretase, whereas depletion of C/EBPβ abrogates AD pathologies through by δ-secretase expression (16). C/EBPs are implicated in inflammation in various neurodegenerative diseases (21–23) and brain injury (24). Moreover, C/EBPs are up-regulated in AD (25, 26). Notably, C/EBPβ has been reported to mediate learning and memory (27).

In the current study, we report that C/EBPβ/δ-secretase axis instigates Aβ aggregation and Tau hyperphosphorylation in a spatiotemporal manner in a 3×Tg AD mouse model. The up-regulated δ-secretase simultaneously cleaves both APP and Tau, and the subsequent APP C586 and Tau N368 truncations act as earlier precipitating events that precede Aβ aggregation. Remarkably, these activities are tightly coupled with aging and mediate neuronal cell death, neuro-inflammation, synaptic dysfunctions, and other disease processes. Strikingly, the C/EBPβ/δ-secretase axis also temporally dictates both APP and Tau mRNA transcription. Inactivation of C/EBPβ or δ-secretase attenuates AD pathologies in 3×Tg mice, restoring cognitive functions.

Results

The C/EBPβ/δ-Secretase Axis Is Escalated in 3×Tg Mice in an Age-Dependent Way. 3×Tg AD mice harboring the $PS1_{M146V}$, APP_{Swe}, and Tau $_{P301L}$ transgenes, which are under the control of mouse Thy1.2 regulatory element, progressively develop both senile plaques and NFT (28, 29). To explore the biological roles of the C/EBPβ/δ-secretase axis in these events spatiotemporally, we performed immunohistochemistry (IHC) on brain sections from the prefrontal cortex (PFC) and hippocampus (HC) of 3×Tg mice of different ages with anti-C/EBPβ or anti-AEP, respectively. C/EBPβ and δ- PFC secretase were escalated in an age-dependent manner in both brain regions, with C/EBPβ residing mainly in the nucleus and δ-secretase in the cytoplasm (Fig. 1*A*). Quantitative analysis of the signal intensities revealed significant augmentation of both proteins in the aged groups (Fig. 1*B*). Immunoblotting further validated the age-dependent up-regulation patterns. Consequently, the truncated products downstream from δ-secretase including APP N373, N585, and Tau N368 exhibited the similar format, fitting with the gradually elevated δ-secretase levels. Accordingly, Tau hyperphosphorylation AT8 signals were steadily increased. Interestingly, human Tau (HT7) and total Tau (human and mouse Tau, Tau5) were also escalated temporally (Fig. 1*C*), suggesting that the Thy1 promoter may be activated progressively as well. Noticeably, caspase-3 was activated in the 3×Tg mouse brain (Fig. 1*C*, 10th blot), indicating that apoptosis is instigated gradually with age. As expected, qRT-PCR analysis showed that the mRNA levels of C/EBPβ, δ-secretase (*LGMN*), and Tau (*MAPT*) genes were in alignment with their protein concentrations. Remarkably, human APP mRNAs were also increased in an age-dependent way, although the total protein levels showed no evident change the brains of different ages (Fig. 1*D*). The δ-secretase enzymatic assay demonstrated that AEP activities were augmented temporally (Fig. 1*E*). Hence, the C/EBPβ/δ-secretase axis is up-regulated in an age-dependent manner in 3×Tg mice.

Knockout of C/EBPβ/δ-Secretase Decreases APP and Tau Expression and Proteolytic Cleavage. Since some of C/EBP$\beta^{-/-}$ mouse strains are lethal or possess abnormal and severe phenotypes, we chose to use C/EBP$\beta^{+/-}$ mice instead of the homozygous mice. To investigate the pathological effects of the C/EBPβ/δ-secretase axis in amyloidogenic and Tau pathologies, we

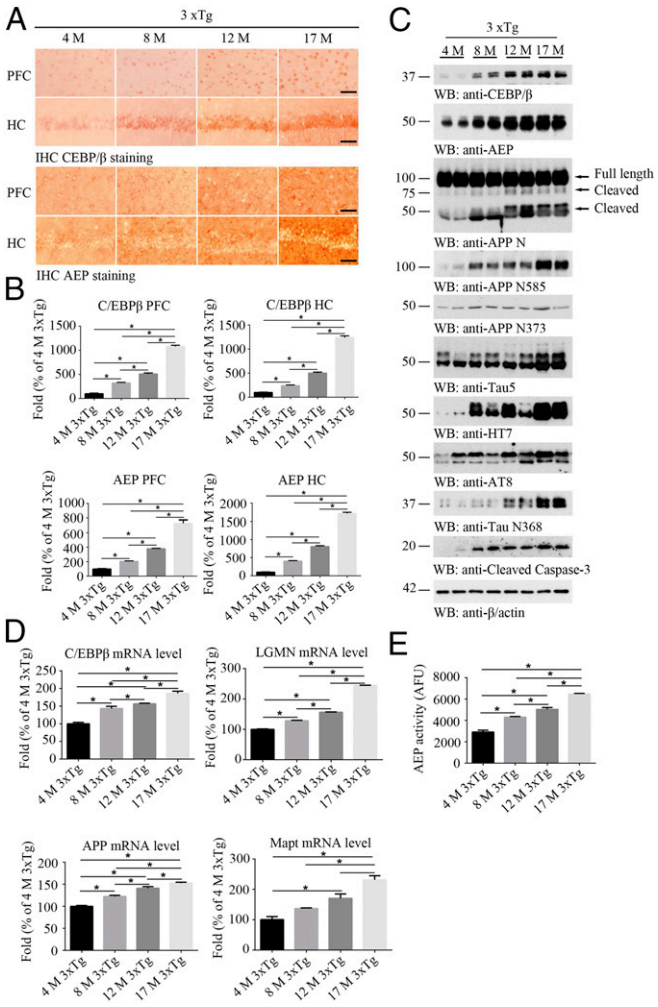

Fig. 1. C/EBPβ/δ-secretase is escalated in an age-dependent way. (*A* and *B*) IHC (*A*) and quantification (*B*) of C/EBPβ and δ-secretase in PFC and HC. Data represent the mean ± SEM of nine sections from three samples in each group; $*P < 0.05$, one-way ANOVA. (Scale bars, 50 μm.) (*C*) Western blots (WB) showing C/EBPβ, AEP, cleaved caspase-3, APP, and Tau expression and processing in 3×Tg mouse brains during aging. (*D*) mRNAs of C/EBPβ, LGMN, APP, and MAPT were analyzed by real-time PCR. Data represent the mean ± SEM of three samples, $*P < 0.05$, one-way ANOVA. (*E*) AEP activity assay in the brain samples. Data represent the mean ± SEM of three samples; $*P < 0.05$, one-way ANOVA.

crossed C/EBP$\beta^{+/-}$ or AEP$^{-/-}$ mice with 3×Tg AD mice and obtained 3×Tg/C/EBP$\beta^{+/-}$ mice and 3×Tg/AEP$^{-/-}$ mice, respectively. Consequently, IHC analysis showed that C/EBPβ and δ-secretase were significantly reduced in both the PFC and HC regions of these mice (Fig. 2 *A* and *B*). Immunoblotting also validated these observations. Accordingly, APP N585, N373, and Tau N368 were robustly diminished when either C/EBPβ or δ-secretase was depleted from 3×Tg mice, as was the expression of Tau (as recognized by both HT7 and Tau5) and its hyperphosphorylated version (AT8). Notably, caspase-3 activation was substantially repressed when C/EBPβ or δ-secretase was eradicated (Fig. 2*C*), suggesting that activation of the C/EBPβ/δ-secretase axis somehow mediates the apoptosis in 3×Tg mice. It is worth noting that C/EBPβ and LGMN mRNA levels were strongly attenuated in both 3×Tg/C/EBP$\beta^{+/-}$ and 3×Tg/AEP$^{-/-}$ mice, suggesting that δ-secretase, the downstream target of C/EBPβ, somehow also feeds back to mediate C/EBPβ expression as well. Noticeably, both APP and MAPT mRNAs were attenuated, when C/EBPβ or δ-secretase

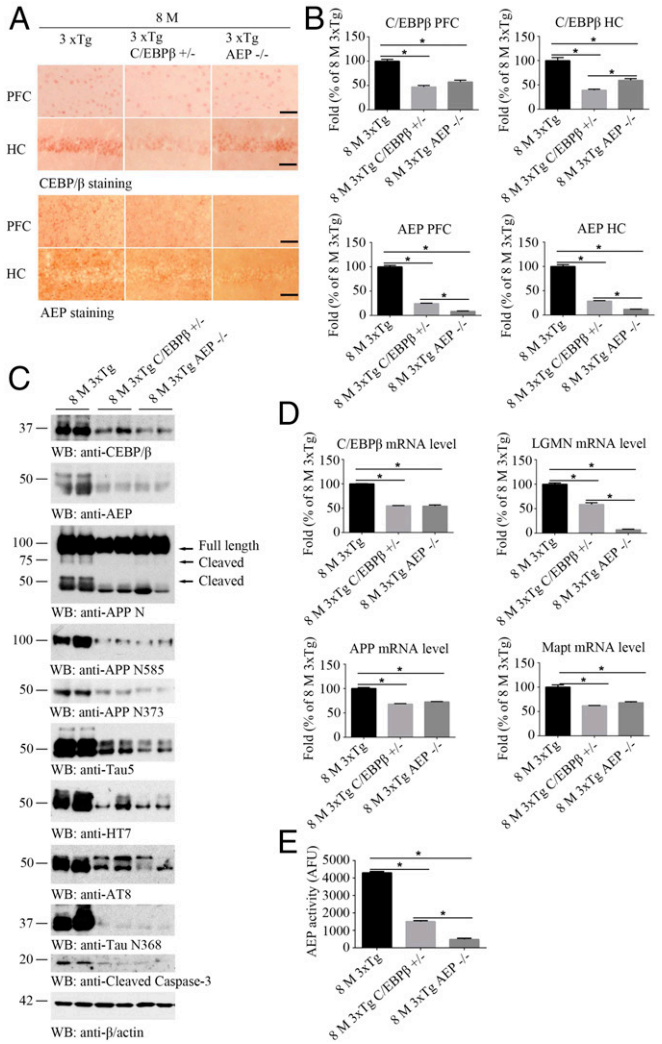

Fig. 2. Knockout of C/EBPβ/δ-secretase in 3×Tg mice decreases APP and Tau expression and proteolytic cleavage. (*A* and *B*) IHC (*A*) and quantification (*B*) of C/EBPβ and δ-secretase in the PFC and HC. Data represent the mean ± SEM of nine sections from three samples in each group; $*P < 0.05$, one-way ANOVA. (Scale bars, 50 μm.) (*C*) Western blots showing C/EBPβ, AEP, cleaved caspase-3, APP, and Tau expression and processing in mouse brains. (*D*) mRNAs of C/EBPβ, LGMN, APP, and MAPT were analyzed by real-time PCR. (*E*) AEP activity assay in the brain samples. Data represent the mean ± SEM; representative data of three samples; $*P < 0.05$ compared with 8-mo-old 3×Tg mice, one-way ANOVA.

was depleted in 3×Tg mice (Fig. 2*D*). As expected, AEP enzymatic activity was strongly reduced in 3×Tg/C/EBPβ$^{+/-}$ mice compared with 3×Tg mice and was completely eliminated in 3×Tg/AEP$^{-/-}$ mice (Fig. 2*E*). Thus, the C/EBPβ/δ-secretase axis modulates both APP and Tau expression and their proteolytic fragmentation.

Knockout of C/EBPβ/δ-Secretase in 3×Tg Mice Attenuates Amyloidogenic Activities. IHC study of Aβ expression in different brain regions including the PFC, HC, basolateral amygdala (BLA), entorhinal cortex (EC), and locus coeruleus (LC) in 3×Tg mice revealed that Aβ signals were augmented in these regions temporally (*SI Appendix*, Fig. S1 *A* and *B*). Aβ ELISA demonstrated that both Aβ40 and Aβ42 were increased in an age-dependent manner (*SI Appendix*, Fig. S1*C*). Thioflavin S and anti-Aβ costaining showed that fibrillar Aβ peptides were aggregated in the PFC and HC regions of 12- and 17-mo-old 3×Tg mouse brains (*SI Appendix*, Fig. S1*D*). Noticeably, as Aβ signals gradually escalated in 3×Tg mice in an age-dependent manner, the δ-secretase–truncated APP C586 fragment was also progressively elevated in both the PFC and HC (*SI Appendix*, Fig. S1 *E* and *F*). To assess the roles of C/EBPβ/δ-secretase in the amyloidogenic pathway, we conducted Aβ IHC staining on different brain regions including the PFC, HC, BLA, EC, and LC from 3×Tg/C/EBPβ$^{+/-}$ and 3×Tg/AEP$^{-/-}$ mice. Compared with 3×Tg mice, Aβ levels were evidently reduced in all these regions in 8-mo-old C/EBPβ- or AEP-depleted mice (Fig. 3 *A* and *B*), indicating that C/EBPβ and δ-secretase are required for amyloid peptide production in 3×Tg mice. Aβ ELISA analysis revealed that both Aβ40 and Aβ42 were significantly decreased in both 3×Tg/C/EBPβ$^{+/-}$ and 3×Tg/AEP$^{-/-}$ mice compared with 3×Tg mice (Fig. 3*C*). To explore further whether Aβ production is correlated with APP fragmentation by δ-secretase, we performed anti-Aβ and anti-APP C586 immunofluorescent costaining on different brain regions. Both Aβ and APP C586 were massive and costained in numerous cells in 8-mo-old 3×Tg brains, and these effects were greatly abrogated in 3×Tg/C/EBPβ$^{+/-}$ and 3×Tg/AEP$^{-/-}$ mice (Fig. 3 *D* and *E*), indicating that the C/EBPβ/δ-secretase axis is indispensable for Aβ production in 3×Tg mice.

Knockout of C/EBPβ/δ-Secretase in 3×Tg Mice Mitigates Tau Hyperphosphorylation. Spatiotemporal analysis of pTau IHC staining signals demonstrated that Tau hyperphosphorylation also

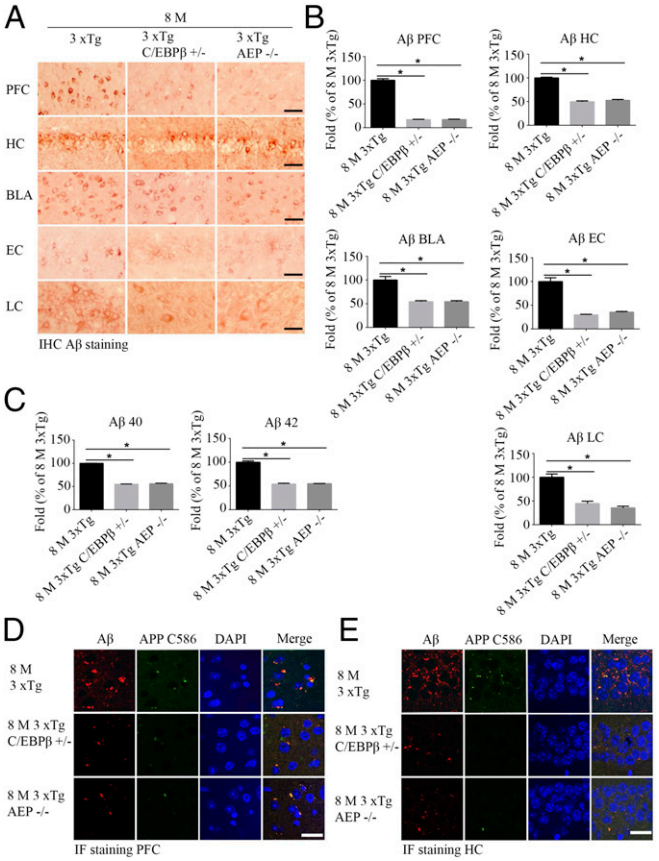

Fig. 3. Knockout of C/EBPβ/δ-secretase in 3×Tg mice attenuates amyloidogenic pathway. (*A* and *B*) Aβ immunostaining (*A*) and quantification (*B*) of the PFC, HC, BLA, EC, and LC. Data represent the mean ± SEM of nine sections from three mice in each group; $*P < 0.05$, one-way ANOVA. (Scale bars, 50 μm.) (*C*) Quantification of Aβ 1–40 and Aβ 1–42 levels by ELISA. Data represent the mean ± SEM of three mice per group; $*P < 0.05$, one-way ANOVA. (*D* and *E*) Immunofluorescent staining of Aβ and cleaved APP C586 in the PFC (*D*) and HC (*E*) in 3×Tg mice. (Scale bars, 20 μm.)

occurred in different brain regions of 3×Tg mice in an age-related pattern (*SI Appendix*, Fig. S2 *A* and *B*). In addition, histological stains, such as Gallyas silver staining, also identified altered Tau-reactive neurons, indicating that some of the accumulated Tau proteins form aggregates progressively in different brain regions (*SI Appendix*, Fig. S2*C*). Immunofluorescent costaining of AT8- and δ-secretase–truncated Tau N368 fragments showed that the AT8 and Tau N368 signals correlated tightly with each other and increased gradually in different brain regions (*SI Appendix*, Fig. S2 *D–F*). Since Tau pathologies in AD are first initiated from LC neurons, we monitored Tau cleavage and phosphorylation in the LC. In the LC region, AT8 activities were augmented in tyrosing hydroxylase (TH)-positive norepinephrine neurons in an age-related manner (*SI Appendix*, Fig. S2*G*). Our previous study showed that Tau N368 cleavage by δ-secretase mediates Tau phosphorylation status (11). Accordingly, diminishing δ-secretase by depleting its upstream C/EBPβ or knocking out the *LGMN* gene from 3×Tg mice significantly repressed Tau hyperphosphorylation in various brain regions in 3×Tg/C/EBPβ$^{+/-}$ and 3×Tg/AEP$^{-/-}$ mice compared with 3×Tg mice (Fig. 4 *A* and *B*). Again, the robust signals that were costained in 8-mo-old 3×Tg mice were strongly decreased in 3×Tg/C/EBPβ$^{+/-}$ and 3×Tg/AEP$^{-/-}$ mice (Fig. 4 *C–F*), further supporting the notion that Tau proteolytic cleavage by δ-secretase is required for Tau hyperphosphorylation. Moreover, NeuN and TUNEL costaining on HC sections showed extensive neuronal apoptosis leading to massive neuronal cell loss in 3×Tg mice compared with 3×Tg/C/EBPβ$^{+/-}$ and 3×Tg/AEP$^{-/-}$ mice (Fig. 4*G*). Hence, depletion of the C/EBPβ/δ-secretase axis represses Tau phosphorylation and aggregation, resulting in suppression of neuronal loss in 3×Tg mice.

Knockout of C/EBPβ/δ-Secretase in 3×Tg Mice Diminishes Neuroinflammation and Rescues Cognitive Functions. Previous studies show that C/EBPβ is mainly activated by inflammation and Aβ (20, 21). To explore whether neuroinflammation is age related in 3×Tg mice, we conducted an Iba1 IHC study in both the PFC and HC regions and found that microglia cells were age-dependently activated (*SI Appendix*, Fig. S3*A*). Quantitative ELISA analysis showed that inflammatory cytokines, including IL-1β, IL-6, and TNFα, in 3×Tg mice were augmented gradually in an age-dependent manner (*SI Appendix*, Fig. S3*B*). Accompanying escalating neuroinflammation, NeuN and TUNEL costaining revealed that hippocampal neuronal apoptosis was progressively elevated, resulting in substantial neuronal loss in aged 3×Tg mice (*SI Appendix*, Fig. S3*C*). Moreover, Golgi staining showed that the dendritic spines were steadily reduced in aged 3×Tg mice (*SI Appendix*, Fig. S4*A*). EM analysis found that the synapses were also significantly decreased in an age-dependent manner in 3×Tg mice (*SI Appendix*, Fig. S4*B*), consistent with the gradually declining cognitive functions demonstrated in both fear-conditioning and Morris water maze behavioral tests (*SI Appendix*, Fig. S4 *C* and *D*).

To interrogate the pathological roles of the C/EBPβ/δ-secretase axis in these events, we monitored microglia cell activation in both the PFC and HC in 3×Tg/C/EBPβ$^{+/-}$ and 3×Tg/AEP$^{-/-}$ mice. Compared with 8-mo-old WT 3×Tg mice, Iba1 IHC signals were substantially attenuated when C/EBPβ or δ-secretase was depleted in 3×Tg mice (Fig. 5 *A* and *B*). Once again, inflammatory cytokines were significantly reduced in these mice as compared with WT 3×Tg mice (Fig. 5*C*). EM analysis showed that synapses were increased in 3×Tg/C/EBPβ$^{+/-}$ and 3×Tg/AEP$^{-/-}$ mice compared with 3×Tg mice (Fig. 5*D*). Since pathological Tau aggregation is associated with synaptic dysfunctions (30), we performed Gallyas silver staining and found that fibrillary Tau aggregations were also alleviated in C/EBPβ- or δ-secretase–depleted 3×Tg mice (*SI Appendix*, Fig. S5*A*). In alignment with these findings, Golgi staining demonstrated that dendritic spine numbers were up-regulated in 3×Tg/C/EBPβ$^{+/-}$ and 3×Tg/AEP$^{-/-}$ mice compared with 3×Tg mice (*SI Appendix*, Fig. S5*B*). Consequently, both the fear-conditioning and Morris water maze cognitive behavioral assays revealed that eradication of C/EBPβ or δ-secretase significantly restored learning and memory activities in 3×Tg mice (Fig. 5 *E* and *F*). Therefore, these data support the notion that the C/EBPβ/δ-secretase axis regulates both Aβ and Tau pathologies and mediates the neuroinflammation and neuronal loss in 3×Tg AD mice. Inactivation of this pathway rescues cognitive dysfunctions in the AD mouse model.

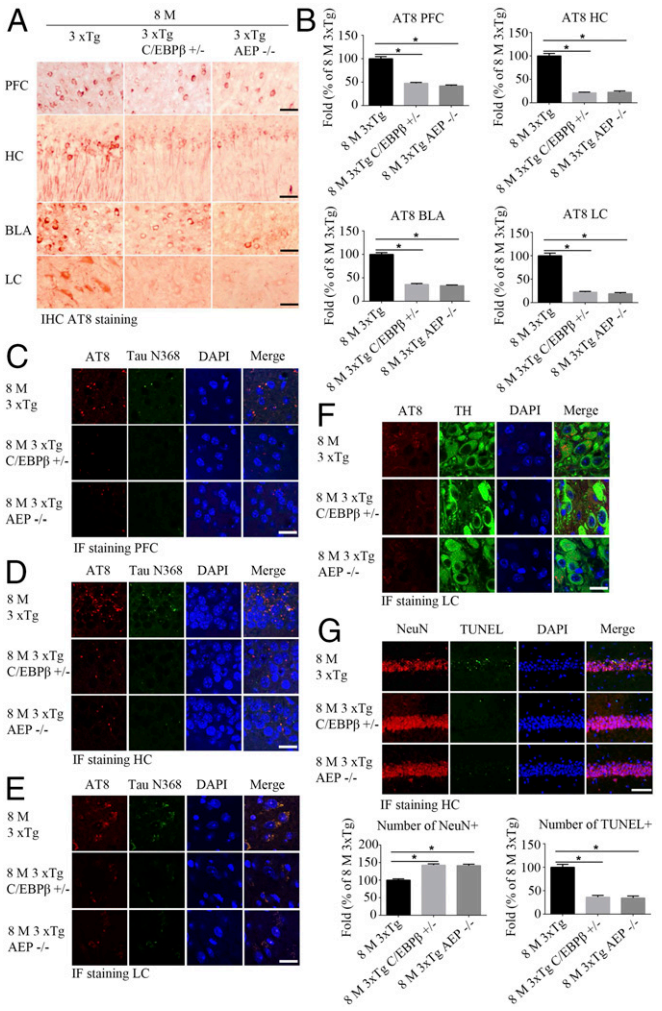

Fig. 4. Knockout of C/EBPβ/δ-secretase in 3×Tg mice mitigates Tau hyperphosphorylation. (*A* and *B*) Tau immunostaining (*A*) and quantification (*B*) of the PFC, HC, BLA, and LC. Data represent the mean ± SEM of nine sections from three mice in each group; **P* < 0.05, one-way ANOVA. (Scale bars, 50 μm.) (*C–E*) Immunofluorescent staining of AT8 and cleaved Tau N368 in the PFC (*C*), HC (*D*), and LC (*E*). (*F*) Immunofluorescent staining of AT8 and TH in the LC. (*G*) Immunofluorescent staining of NeuN and TUNEL in the HC. Data represent the mean ± SEM of nine sections from three mice in each group; **P* < 0.05, one-way ANOVA. (Scale bars, 20 μm.)

Discussion

In the current study, we crossed AEP (δ-secretase)-knockout mice and C/EBPβ$^{+/-}$ mice with 3×Tg mice to dissect the pathological roles of the C/EBPβ/δ-secretase axis in AD pathogenesis. Employing these two different animal models to assess the AD-related pathologies of 3×Tg mice at different ages, we explored the spatial and temporal relationship between activation of the C/EBPβ/δ-secretase axis and its effects in AD pathologies.

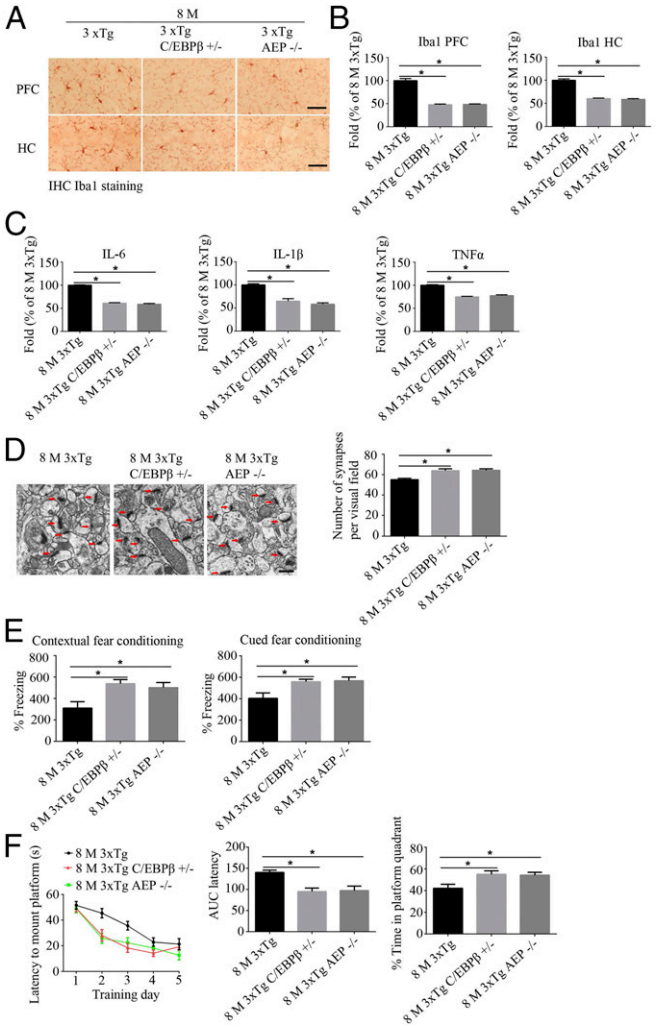

Fig. 5. Knockout of C/EBPβ/δ-secretase diminishes neuroinflammation and rescues cognitive functions. (*A*) Immunostaining of Iba1 in the PFC and HC. (Scale bars, 50 μm.) (*B*) Quantification of Iba-1 immunoreactivities. Data represent the mean ± SEM of nine sections from three mice in each group; $*P < 0.05$, one-way ANOVA. (*C*) Reduction of C/EBPβ and knockdown of δ-secretase decreases the expression levels of inflammatory cytokines in 3×Tg mice. Data represent the mean ± SEM of three mice per group; $*P < 0.05$, one-way ANOVA. (*D*) EM (*Left*) and quantification (*Right*) of synapses. Arrows indicate the synapses ($n = 8$ per group). Data represent the mean ± SEM; $*P < 0.05$, one-way ANOVA. (Scale bar, 0.5 μm.) (*E*) Fear-conditioning tests. Data represent the mean ± SEM of $n = 8$ mice per group; $*P < 0.05$, one-way ANOVA. (*F*) Morris water maze analysis of time to platform (*Left*) and integrated latency (area under the curve; AUC) of mice (*Center*). (*Right*) Probe trail result. Data represent the mean ± SEM of $n = 8$ per group; $*P < 0.05$, one-way ANOVA.

Interestingly, C/EBPβ could also mediate both APP and Tau transcriptive expression. We showed that both C/EBPβ and its downstream effector δ-secretase are escalated age-dependently in different brain regions in 3×Tg AD mice, consistent with APP N373, N583, and Tau N368 proteolytic fragmentation by active δ-secretase. Moreover, we found that δ-secretase–cleaved APP C-terminal fragment C586–696 and Tau N368 tightly correlated with Aβ and AT8 activities, respectively. Partial deletion of C/EBPβ or knockout of δ-secretase in 3×Tg mice substantially blunted the production of APP C586 and Tau N368 truncates, robustly inhibiting Aβ or AT8 signals, supporting the notion that δ-secretase cleavage of both APP and Tau plays a key role in triggering AD pathogenesis. Furthermore, we also found that neuroinflammation and neuronal cell loss were potently attenuated in 3×Tg/C/EBPβ$^{+/-}$ and 3×Tg/AEP$^{-/-}$ mice compared with 3×Tg mice, leading to augmentation of synapses and restoration of learning and memory in aged 3×Tg mice.

In a previous study, Oddo et al. (29) showed that Aβ occurs in the cortex and hippocampus of 3×Tg mice at age 4–5 mo, much earlier than Tau pathologies (at age ∼12 mo), suggesting that these findings support the amyloid cascade hypothesis. However, we and others found that Tau pathologies are demonstrable as early as age 4 mo (Fig. 3) or even as early as age 3 wk and increase with age in different brain regions (31). Presumably, amyloid might not act as a trigger for Tau pathologies, at least in the 3×Tg mouse model. Mounting evidence challenges this overly simplified one-way amyloid–Tau degenerative cascade. For example, many cognitively normal elderly individuals display relatively large amounts of Aβ in their brains (32, 33). Recently, imaging Aβ with PET tracer studies in cognitively normal subjects showed that almost one-third of aged people exhibit major amounts of Aβ in their brains (34, 35). Furthermore, intraneuronal Tau alterations precede aggregated Aβ deposition in the presymptomatic stages (Braak stage 1–3) of AD (36), and Tau tangles develop temporally either before or independently of Aβ plaques (37–39). Moreover, greater Aβ deposition and NFT-like formation with increased neuronal loss was found in double-transgenic mice expressing both human mutant Tau and APP than in single-transgenic mice expressing APP or Tau, suggesting that Tau might accelerate amyloid deposition (40). Recently, it has been reported that human secreted Tau increases Aβ production in human neurons (41). Taken together, these findings suggest that the causal link between aberrant APP processing and Tau alterations remains controversial.

C/EBPβ-binding sites have been identified in numerous cytokines and proinflammatory genes (19). In addition to promoting the production of inflammatory mediators, C/EBP family members are themselves induced by the classic proinflammatory triad of IL-1β, IL-6, and TNF-α (17–19), all of which are significantly increased in pathologically impacted regions of the AD brain (42). Moreover, it has been reported that Aβ activates C/EBPβ (20). This is consistent with the finding that C/EBPβ is upregulated in human AD brains (25, 26). Aβ and IL-6 additively increase C/EBPβ activity (43). Hence, there is a feedback loop between amyloid and neuroinflammation via C/EBPβ activation in microglia or astrocytes. Noticeably, we also found that both APP and MAPT mRNA are progressively augmented in 3×Tg mice (Fig. 1*D*) and are significantly diminished in 3×Tg/C/EBPβ$^{+/-}$ and 3×Tg/AEP$^{-/-}$ mice (Fig. 2*D*), supporting the notion that the C/EBPβ/δ-secretase axis is required for the upregulation of both APP and Tau expression. In 3×Tg mice, both human APP and MAPT transgenes are under the regulation of the Thy1 promoter (29). Promoter DNA sequence analysis demonstrated that the Thy1 promoter contains numerous transcriptional factor-binding motifs, including C/EBPβ-binding sites, supporting the observations that both human APP and MAPT mRNA transcription oscillates with C/EBPβ levels. Probably, C/EBPβ may act as a transcription factor for both APP and MAPT, dictating their up-regulation in AD pathogenesis. On the other hand, we have shown that δ-secretase also feeds back and represses C/EBPβ expression in 3×Tg/AEP$^{-/-}$ mice (Fig. 2 *A–D*), explaining why human APP and MAPT transgenes are also attenuated in 3×Tg/AEP$^{-/-}$ mice. Further, both Aβ and neuroinflammation are decreased in 3×Tg/AEP$^{-/-}$ mice, resulting in the suppression of C/EBPβ activity. Conceivably, under various risk factors including ApoE4, traumatic brain injury, diabetes, or the stress caused by chronic cerebral hypoperfusion, the C/EBPβ/δ-secretase axis may be constantly activated and amplified in the brain. This axis increases the protein levels of both substrates of APP and Tau, which are proteolytically truncated by δ-secretase. These processes will disturb Aβ

homeostasis, facilitating Aβ oligomerization and fibrillar aggregation. On the other hand, truncated Tau N368 looses its microtubule-binding activity and is prone to be hyperphosphorylated and aggregated into NFTs, leading to defects in synaptic plasticity and neurotoxicities (11). Since both α-synuclein and TDP-43 are also proteolytic substrates of δ-secretase (44, 45), the aggregation of these toxic proteins may initiate at this stage. At this point, the cascade might be set in full motion, as neuronal loss, oxidative damage, inflammation, and clinical symptoms become evident, and neutralizing or removing Aβ is less likely to exhibit a major effect, perhaps explaining why anti-Aβ therapy keeps failing.

δ-Secretase activation requires sequential autocleavage of C-terminal N323 and subsequent truncation at D25, which is mediated by caspases (7). Our previous study showed that δ-secretase is implicated in neuronal cell death initiated by stroke. δ-Secretase is activated under acidosis during the ischemia, and active δ-secretase cuts SET at N175, alleviating its inhibition on DNase, leading to substantial genomic DNA nicking and neuronal cell death (10). Interestingly, we found that both caspase-3 and δ-secretase are progressively activated in 3×Tg mice (Fig. 1*C*), coupled with gradual up-regulation of neuronal apoptosis in the HC of 3×Tg (*SI Appendix*, Fig. S3*C*). Presumably, active caspase-3 may cleave δ-secretase at D25, stimulating its enzymatic augmentation, which subsequently provokes both APP N373 and N585 and Tau N368 proteolytic cleavage. δ-Secretase is highly expressed in the kidney (46), and its expression level in the brain is age-related (11). Knockout of δ-secretase leads to late endosomes and lysosomes augmentation and dislocation from the apical region of the kidney-proximal tubule cells and to the abnormal lysosomes contained in electron-dense and/or membranous materials (46). Nonetheless, AEP-null mice are viable and fertile without any demonstrable abnormal defects from the development stage to adulthood. They display normal cognitive function and brain structures (47, 48). Recently, we have identified a small molecule that selectively targets δ-secretase. Chronic treatment of 5×FAD mice and Tau P301S mice strongly inhibited amyloid pathologies and tauopathies, rescuing the cognitive impairments. Moreover, no demonstrable side effects were observed in these animals (15), supporting the notion that δ-secretase might be an attractive drug target for treating AD and other neurodegenerative diseases, including Parkinson disease (PD) and amyotrophic lateral sclerosis. We have reported that α-synuclein and TDP-43 are also δ-secretase substrates as well; the proteolytic cleavage occurs in human patient brains and mediates the onset of their pathogenesis (44, 45). Together, our findings strongly suggest that the C/EBPβ/δ-secretase axis plays a critical role in manipulating AD pathogenesis and that inhibition of δ-secretase might provide an unprecedently successful disease-modifying strategy in slowing down AD progression.

Materials and Methods

Mice. 3×Tg mice were ordered from the Jackson Laboratory (34830). Since some of the homozygous mutations are lethal on pure-strain backgrounds, C/EBPβ mice were maintained as heterozygotes on two separate strain backgrounds (C57BL/6 and 129Sv). These two strains were crossed to generate viable F1 hybrid WT and C/EBPβ$^{-/-}$ littermates, which were used for aging studies. AEP-knockout mice on a mixed C57BL/6 and 129/Ola background were generated as reported (46). The following animal groups were analyzed: 3×Tg, 3×Tg/C/EBPβ$^{+/-}$, and 3×Tg/AEP$^{-/-}$. Both female and male mice were used. Animal care and handling were performed according to NIH animal care guidelines and the Declaration of Helsinki and Emory Medical School guidelines. The protocol was reviewed and approved by the Emory Institutional Animal Care and Use Committee.

Antibodies and Reagents. Antibodies to the following targets were used: antibody to C/EBPβ (Santa Cruz); AEP antibody clone 6E3 and 11b7 (from Colin Watts, University of Dundee, Dundee, UK); anti-APP N-terminal antibody (Calbiochem); APP N585, APP N373, APP C586, and Tau N368, which respectively specifically recognize the δ-secretase–derived APP and tau fragments and were described previously (11, 12); tau5 (Thermo Fisher Scientific); HT7 (Thermo Fisher Scientific); AT8 (Thermo Fisher Scientific); cleaved caspase-3 (Cell Signaling); β-actin (Cell Signaling); Aβ 4G8 (Sigma); NeuN (Cell Signaling); and TH antibody (Cell Signaling). The TUNEL in situ cell death detection kit was from Roche. Human Aβ40, Aβ42, and inflammatory cytokine ELISA kits were purchased from Invitrogen. All chemicals not mentioned above were purchased from Sigma-Aldrich.

AEP Activity Assay. Tissue homogenates (10 μg) were incubated in 200 μL of reaction buffer (20 mM citric acid, 60 mM Na_2HPO_4, 1 mM EDTA, 0.1% CHAPS, and 1 mM DTT, pH 5.5) containing 20 μM AEP substrate Z-Ala-Ala-Asn-AMC (Bachem). AMC released by substrate cleavage was quantified by measuring at 460 nm in a fluorescence plate reader at 37 °C in kinetic mode.

ELISA Quantification of Aβ and Inflammatory Cytokine. To detect the concentration of Aβ in tissues lysates, the samples were diluted with cold reaction buffer (PBS with 5% BSA and 0.03% Tween-20, supplemented with protease inhibitor mixture), centrifuged at 16,000 × *g* for 20 min at 4 °C, and analyzed with human Aβ1-40 and Aβ1-42 ELISA kits according to the manufacturer's instructions. For the quantification of inflammatory cytokine, tissues lysates were analyzed with mouse IL-6, IL-1β, and TNF-α ELISA kits according to the manufacturer's instructions. The sample concentrations were determined by comparison with the standard curve.

Real-Time PCR. mRNA levels were analyzed by real-time, qPCR. RNA was isolated by TRIzol (Life Technologies). Reverse transcription was performed with SuperScript III reverse transcriptase (Life Technologies). Gene-specific primers and probes were designed and bought from Taqman (Life Technologies). All real-time PCR reactions were performed using the ABI 7500-Fast Real-Time PCR System and the Taqman Universal Master Mix Kit (Life Technologies). The relative quantification of gene expression was calculated using the ΔΔCt method. For each data point, at least duplicate wells were used. Each experiment was repeated at least three times.

Western Blot Analysis. Mouse brain tissue were lysed in lysis buffer [50 mM Tris (pH 7.4), 40 mM NaCl, 1 mM EDTA, 0.5% Triton X-100, 1.5 mM Na_3VO_4, 50 mM NaF, 10 mM sodium pyrophosphate, and 10 mM sodium β-glycerophosphate, supplemented with a protease inhibitors mixture] and centrifuged for 15 min at 16,000 × *g*. The supernatant was boiled in SDS loading buffer. After SDS/PAGE, the samples were transferred to a nitrocellulose membrane. Primary antibodies to the following targets were used: antibody to C/EBPβ (1:1,000); AEP antibody clone 6E3 (1:1,000); APP N (1:1,000); APP N585 (1:1,000); APP N373(1:1,000); tau5 (1:1,000); HT7 (1:1,000); AT8 (1:1,000); Tau N368 (1:1,000); cleaved caspase-3 (1:1,000); and β-actin (1:5,000).

IHC. For IHC staining, the brain sections were treated with 0.3% H_2O_2 for 10 min. Then sections were washed three times in PBS and blocked in 1% BSA and 0.3% Triton X-100, for 30 min followed by overnight incubation with anti-C/EBPβ (1:500), AEP antibody clone 11B7 (1: 500), Aβ antibody (1:500), and AT8 (1:500) at 4 °C. The signal was developed using the Histostain-SP kit (Thermo Fisher Scientific). For immunofluorescence staining, the sections were incubated overnight at 4 °C with primary Aβ (1:500), APP C586 (1:1,000), AT8 (1:500), Tau N368 (1:1,000), and TH antibody (1:500) antibodies. After washing with Tris-buffered saline, the sections were incubated with a mixture of Alexa Fluor 488- and 594-coupled secondary antibodies (Invitrogen) for detection. DAPI (1 μg/mL) (Sigma) was used for staining nuclei. Images were acquired with an Olympus confocal FV1000 imaging system. ImageJ (NIH) was used for intensity and colocalization analysis.

Gallyas Silver Staining. Silver staining was performed using the Gallyas method. Brain sections (30 μm) were incubated in 5% periodic acid for 5 min, washed in water, and then placed in alkaline silver iodide solution (containing 1% silver nitrate) for 1 min. The sections were then washed in 0.5% acetic acid for 10 min, placed in developer solution for 15 min, and washed with 0.5% acetic acid and then with water. The sections were treated with 0.1% gold chloride for 5 min, washed in water, and incubated in 1% sodium thiosulfate (hypo) for 5 min before a final washing.

Thioflavin-S Staining. Amyloid plaques were stained with Thioflavin-S. Free-floating 30-μm brain sections were incubated in 0.25% potassium permanganate solution for 20 min, rinsed in distilled water, and incubated in bleaching solution containing 2% oxalic acid and 1% potassium metabisulfite for 2 min. After rinsing in distilled water, the sections were transferred to blocking solution containing 1% sodium hydroxide and 0.9% hydrogen peroxide for 20 min. The sections were incubated for 5 s in 0.25%

acidic acid, washed in distilled water, and stained for 5 min with 0.0125% Thioflavin-S in 50% ethanol. The sections were washed with 50% ethanol and placed in distilled water. Then the sections were covered with a glass cover using mounting solution and were examined under a fluorescence microscope.

EM. After deep anesthesia, mice were perfused transcardially with 2% glutaraldehyde and 3% paraformaldehyde in PBS. Hippocampal slices were postfixed in cold 1% OsO_4 for 1 h. Samples were prepared and examined using standard procedures. Ultrathin sections (90 nm) were stained with uranyl acetate and lead acetate and viewed at 100 kV in a JEOL 200CX electron microscope. Synapses were identified by the presence of synaptic vesicles and postsynaptic densities.

Golgi Stain. Mouse brains were fixed in 10% formalin for 24 h and then were immersed in 3% potassium bichromate for 3 d in the dark. The solution was changed each day. Then the brains were transferred into 2% silver nitrate solution and incubated for 24 h in the dark. Vibratome sections were cut at 60 μm, air dried for 10 min, dehydrated through 95% and 100% ethanol, cleared in xylene, and coverslipped.

Morris Water Maze. 3×Tg, 3×Tg/C/EBPβ$^{+/-}$, and 3×Tg/AEP$^{-/-}$ mice at different ages were trained in a round, water-filled tub (52-inch diameter) in an environment rich with extra maze cues. An invisible escape platform was located in a fixed spatial location 1 cm below the water surface independent of the subject's start position on a particular trial. In this manner, subjects needed to utilize extra maze cues to determine the platform's location. At the beginning of each trial, the mouse was placed in the water maze with its paws touching the wall at one of four different starting positions (N, S, E, W). Each subject was given four trials/d for five consecutive days with a 15-min intertrial interval. The maximum trial length was 60 s; if the subject did not reach the platform in the allotted time, it was manually guided to the platform. Upon reaching the invisible escape platform, the subject was left on the platform for an additional 5 s to allow it to survey of the spatial cues in the environment to guide future navigation to the platform. After each trial, the subject was dried and kept in a dry plastic holding cage filled with paper towels to allow the subjects to dry off. The temperature of the water was between 22 and 25 °C. Following the 5 d of task acquisition, a probe trial was presented during which the platform was removed, and the percentage of time spent in the quadrant which previously contained the escape platform during task acquisition was measured over 60 s. All trials were analyzed for latency and swim speed by means of MazeScan (Clever Sys, Inc.).

Contextual Fear Conditioning. The ability to form and retain an association between an aversive experience and environmental cues was tested with a standard fear-conditioning paradigm that occurred over a period of 3 d. The mouse was placed in the fear-conditioning apparatus (7 in wide × 7 in deep × 12 in high; Coulbourn) composed of Plexiglas with a metal shock grid floor and were allowed to explore the enclosure for 3 min. Following this habituation period, three conditioned stimulus (CS)–unconditioned stimulus (US) pairings were presented with a 1-min intertrial interval. The CS was composed of a 20-s, 85-dB tone, and the US was composed of a 2-s 0.5-mA footshock, which was coterminate with each CS presentation. One minute following the last CS–US presentation, the mouse was returned to its home cage. On day 2, the mouse was presented with a context test during which the subject was placed in the same chamber used during conditioning on day 1, and the amount of freezing was recorded via a camera and software provided by Coulbourn. No shocks were given during the context test. On day 3, a tone test was presented during which the subject was exposed to the CS in a novel compartment. Initially, the animal was allowed to explore the novel context for 2 min. Then the 85-db tone was presented for 6 min, and the amount of freezing behavior was recorded.

Statistical Analysis. All data are expressed as the mean ± SEM of three or more independent experiments. The level of significance between groups was assessed with one-way ANOVA followed by the least-significant-difference post hoc test. A value of $P < 0.05$ was considered statistically significant.

ACKNOWLEDGMENTS. We thank the Goizueta Alzheimer's Disease Research Center at Emory University for samples from human PD and dementia with Lewy body patients and healthy controls. This work was supported by NIH Grants R01 NS082338 and RF1 AG05381 (to K.Y.). H.W. is financially supported by the International Postdoctoral Exchange Fellowship Program of the Office of China Postdoctoral Council.

1. De Strooper B, Karran E (2016) The cellular phase of Alzheimer's disease. *Cell* 164: 603–615.
2. Hardy J, Selkoe DJ (2002) The amyloid hypothesis of Alzheimer's disease: Progress and problems on the road to therapeutics. *Science* 297:353–356.
3. Karran E, De Strooper B (2016) The amyloid cascade hypothesis: Are we poised for success or failure? *J Neurochem* 139:237–252.
4. Holmes C, et al. (2008) Long-term effects of Abeta42 immunisation in Alzheimer's disease: Follow-up of a randomised, placebo-controlled phase I trial. *Lancet* 372: 216–223.
5. Lahiri DK, Maloney B, Long JM, Greig NH (2014) Lessons from a BACE1 inhibitor trial: Off-site but not off base. *Alzheimers Dement* 10(5, Suppl):S411–S419.
6. Musiek ES, Holtzman DM (2015) Three dimensions of the amyloid hypothesis: Time, space and 'wingmen'. *Nat Neurosci* 18:800–806.
7. Li DN, Matthews SP, Antoniou AN, Mazzeo D, Watts C (2003) Multistep autoactivation of asparaginyl endopeptidase in vitro and in vivo. *J Biol Chem* 278:38980–38990.
8. Basurto-Islas G, Grundke-Iqbal I, Tung YC, Liu F, Iqbal K (2013) Activation of asparaginyl endopeptidase leads to tau hyperphosphorylation in Alzheimer disease. *J Biol Chem* 288:17495–17507.
9. Lunde NN, et al. (2017) Increased levels of legumain in plasma and plaques from patients with carotid atherosclerosis. *Atherosclerosis* 257:216–223.
10. Liu Z, et al. (2008) Neuroprotective actions of PIKE-L by inhibition of SET proteolytic degradation by asparagine endopeptidase. *Mol Cell* 29:665–678.
11. Zhang Z, et al. (2014) Cleavage of tau by asparagine endopeptidase mediates the neurofibrillary pathology in Alzheimer's disease. *Nat Med* 20:1254–1262.
12. Zhang Z, et al. (2015) Delta-secretase cleaves amyloid precursor protein and regulates the pathogenesis in Alzheimer's disease. *Nat Commun* 6:8762.
13. Wang ZH, et al. (2017) Delta-secretase phosphorylation by SRPK2 enhances its enzymatic activity, provoking pathogenesis in Alzheimer's disease. *Mol Cell* 67:812–825.e5.
14. Wang ZH, et al. (2018) BDNF inhibits neurodegenerative disease-associated asparaginyl endopeptidase activity via phosphorylation by AKT. *JCI Insight* 3:99007.
15. Zhang Z, et al. (2017) Inhibition of delta-secretase improves cognitive functions in mouse models of Alzheimer's disease. *Nat Commun* 8:14740.
16. Wang ZH, et al. (2018) C/EBPβ regulates delta-secretase expression and mediates pathogenesis in mouse models of Alzheimer's disease. *Nat Commun* 9:1784.
17. Magalini A, et al. (1995) Role of IL-1 beta and corticosteroids in the regulation of the C/EBP-alpha, beta and delta genes in vivo. *Cytokine* 7:753–758.
18. Poli V (1998) The role of C/EBP isoforms in the control of inflammatory and native immunity functions. *J Biol Chem* 273:29279–29282.
19. Wedel A, Ziegler-Heitbrock HW (1995) The C/EBP family of transcription factors. *Immunobiology* 193:171–185.
20. Ramberg V, Tracy LM, Samuelsson M, Nilsson LN, Iverfeldt K (2011) The CCAAT/enhancer binding protein (C/EBP) δ is differently regulated by fibrillar and oligomeric forms of the Alzheimer amyloid-β peptide. *J Neuroinflammation* 8:34.
21. Ejarque-Ortiz A, et al. (2007) Upregulation of CCAAT/enhancer binding protein beta in activated astrocytes and microglia. *Glia* 55:178–188.
22. Cardinaux JR, Allaman I, Magistretti PJ (2000) Pro-inflammatory cytokines induce the transcription factors C/EBPbeta and C/EBPdelta in astrocytes. *Glia* 29:91–97.
23. Tengku-Muhammad TS, Hughes TR, Ranki H, Cryer A, Ramji DP (2000) Differential regulation of macrophage CCAAT-enhancer binding protein isoforms by lipopolysaccharide and cytokines. *Cytokine* 12:1430–1436.
24. Cortés-Canteli M, Wagner M, Ansorge W, Pérez-Castillo A (2004) Microarray analysis supports a role for ccaat/enhancer-binding protein-beta in brain injury. *J Biol Chem* 279:14409–14417.
25. Lukiw WJ (2004) Gene expression profiling in fetal, aged, and Alzheimer hippocampus: A continuum of stress-related signaling. *Neurochem Res* 29:1287–1297.
26. Li R, Strohmeyer R, Liang Z, Lue LF, Rogers J (2004) CCAAT/enhancer binding protein delta (C/EBPdelta) expression and elevation in Alzheimer's disease. *Neurobiol Aging* 25:991–999.
27. Taubenfeld SM, Milekic MH, Monti B, Alberini CM (2001) The consolidation of new but not reactivated memory requires hippocampal C/EBPbeta. *Nat Neurosci* 4: 813–818.
28. Oddo S, Caccamo A, Kitazawa M, Tseng BP, LaFerla FM (2003) Amyloid deposition precedes tangle formation in a triple transgenic model of Alzheimer's disease. *Neurobiol Aging* 24:1063–1070.
29. Oddo S, et al. (2003) Triple-transgenic model of Alzheimer's disease with plaques and tangles: Intracellular Abeta and synaptic dysfunction. *Neuron* 39:409–421.
30. Zhao X, et al. (2016) Caspase-2 cleavage of tau reversibly impairs memory. *Nat Med* 22:1268–1276.
31. Oh KJ, et al. (2010) Staging of Alzheimer's pathology in triple transgenic mice: A light and electron microscopic analysis. *Int J Alzheimers Dis* 2010:780102.
32. Price JL, et al. (2009) Neuropathology of nondemented aging: Presumptive evidence for preclinical Alzheimer disease. *Neurobiol Aging* 30:1026–1036.
33. Davis DG, Schmitt FA, Wekstein DR, Markesbery WR (1999) Alzheimer neuropathologic alterations in aged cognitively normal subjects. *J Neuropathol Exp Neurol* 58: 376–388.
34. Rowe CC, et al. (2007) Imaging beta-amyloid burden in aging and dementia. *Neurology* 68:1718–1725.

35. Rodrigue KM, et al. (2012) β-Amyloid burden in healthy aging: Regional distribution and cognitive consequences. *Neurology* 78:387–395.
36. Braak H, Braak E (1995) Staging of Alzheimer's disease-related neurofibrillary changes. *Neurobiol Aging* 16:271–278, discussion 278–284.
37. Wirths O, Multhaup G, Bayer TA (2004) A modified beta-amyloid hypothesis: Intraneuronal accumulation of the beta-amyloid peptide–The first step of a fatal cascade. *J Neurochem* 91:513–520.
38. Schönheit B, Zarski R, Ohm TG (2004) Spatial and temporal relationships between plaques and tangles in Alzheimer-pathology. *Neurobiol Aging* 25:697–711.
39. Braak H, Zetterberg H, Del Tredici K, Blennow K (2013) Intraneuronal tau aggregation precedes diffuse plaque deposition, but amyloid-β changes occur before increases of tau in cerebrospinal fluid. *Acta Neuropathol* 126:631–641.
40. Ribé EM, et al. (2005) Accelerated amyloid deposition, neurofibrillary degeneration and neuronal loss in double mutant APP/tau transgenic mice. *Neurobiol Dis* 20: 814–822.
41. Bright J, et al. (2015) Human secreted tau increases amyloid-beta production. *Neurobiol Aging* 36:693–709.
42. Akiyama H, et al. (2000) Inflammation and Alzheimer's disease. *Neurobiol Aging* 21: 383–421.
43. Strohmeyer R, Shelton J, Lougheed C, Breitkopf T (2014) CCAAT-enhancer binding protein-β expression and elevation in Alzheimer's disease and microglial cell cultures. *PLoS One* 9:e86617.
44. Zhang Z, et al. (2017) Asparagine endopeptidase cleaves α-synuclein and mediates pathologic activities in Parkinson's disease. *Nat Struct Mol Biol* 24:632–642.
45. Herskowitz JH, et al. (2012) Asparaginyl endopeptidase cleaves TDP-43 in brain. *Proteomics* 12:2455–2463.
46. Shirahama-Noda K, et al. (2003) Biosynthetic processing of cathepsins and lysosomal degradation are abolished in asparaginyl endopeptidase-deficient mice. *J Biol Chem* 278:33194–33199.
47. Chan CB, et al. (2009) Mice lacking asparaginyl endopeptidase develop disorders resembling hemophagocytic syndrome. *Proc Natl Acad Sci USA* 106:468–473, and erratum (2009) 106:468–473.
48. Miller G, Matthews SP, Reinheckel T, Fleming S, Watts C (2011) Asparagine endopeptidase is required for normal kidney physiology and homeostasis. *FASEB J* 25: 1606–1617.